

A Melt-through Model for Chaos Formation on Europa

David P. O'Brien, Paul Geissler, and Richard Greenberg

Lunar and Planetary Laboratory, University of Arizona, Tucson, Arizona 85721-0092

E-mail: obrien@lpl.arizona.edu

Received March 7, 2001; revised October 8, 2001

The character of chaotic terrain on Europa is consistent with its formation by the melting of a thin conducting ice shell from below. Tidal dissipation can provide adequate energy for such a process. For example, only a few percent of Europa's predicted tidal heat, spread over a region 200 km in diameter, can lead to large melt regions within a few tens of thousands of years. Stronger, more localized concentrations result in melt-through in significantly shorter times (i.e., a few hundred years). The time scale for melt-through is shorter than the time scale for the solid-state viscous inflow of ice by several orders of magnitude. In general, modest concentrations of tidal heat can melt ice away faster than viscous inflow, leading to melt-through. A mechanism to transmit these heat concentrations through the ocean is required for this model. Such heat transport could be the result of convective plumes in the ocean driven by seafloor volcanism or by the destabilization of a stratified ocean.

© 2002 Elsevier Science (USA)

Key Words: Europa; satellites of Jupiter; surfaces, satellites; thermal histories.

1. INTRODUCTION

The European surface is extremely young in geological terms (~20 Myr according to Zahnle *et al.* (1998)) due to widespread resurfacing events of two general kinds, (a) tectonic features driven by tidal stresses that cause cracking and subsequent evolution into ridges and bands (Greenberg *et al.* 1998, Hoppa *et al.* 1999, Tufts *et al.* 2000) and (b) chaotic terrain, which appears to currently cover about 40% of the surface (Greenberg *et al.* 1999, Riley *et al.* 2000).

Chaos regions (see Fig. 1) occur in a wide range of lateral scales from as small as can be discerned given limitations of imaging (km-scale), to over 1000 km across (Greenberg *et al.* 1999, Riley *et al.* 2000). A lumpy matrix usually covers most of the area of a patch of chaos. Often, rafts of preexisting terrain survive within this matrix, shifted somewhat relative to their original position. These rafts often contain raised ridges that represent thicker areas of the shell which would have resisted melting (Greenberg *et al.* 1999); their mobility (Spaun *et al.* 1998) suggests the presence of a sublayer of low-viscosity material, such as a liquid water ocean.

Several formation processes have been suggested for chaotic terrain (Carr *et al.* 1998). These interpretations have included icy volcanism, at least for some small patches of chaos (Greeley *et al.* 1998), solid-state convection (Pappalardo *et al.* 1998), brine mobilization within the ice shell (Head and Pappalardo 1999), and melt-through of a thin ice shell over liquid water (Greenberg *et al.* 1999).

Melt-through of the ice shell was dismissed by Pappalardo *et al.* (1999) and Collins *et al.* (2000) in favor of solid-state convection, diapirism, or brine mobilization theories because melting requires more internal heat production than they assumed for Europa and they did not believe that heat could be effectively transported through the ocean. However, Europa's internal heat production is sensitive to several poorly known parameters. Early estimates were used to make the case for the possibility of a liquid water ocean, so to be conservative they tended to the side of minimal heating (Cassen *et al.* 1979, 1980, Squyres *et al.* 1983). However, Europa's tidal heating may be far larger and the shell far thinner than previously believed (Geissler *et al.* 2001). Furthermore, several processes have been proposed which could lead to the propagation of seafloor heat concentrations to the surface. Thomson and Delaney (2001) have proposed a model in which rotationally confined thermal plumes in a weakly stratified ocean can propagate to the base of the shell while spreading only 10–100 km. Kargel *et al.* (2000) have proposed that the destabilization of a hot, stratified ocean could lead to large (both in size and temperature) thermal anomalies at the base of the shell. Further research is necessary to understand these and other potential heat-concentrating processes and determine if they are consistent with the observed size distribution and morphology of chaos features on Europa.

Even if heat can be sufficiently concentrated at the base of the shell, it has been suggested that any local thinning of the ice would be counteracted by viscous ice flow refilling the opening (Stevenson 2000). However, this is based on the assumption of a thick ice shell, which is not the case considered here. Here we show that there may be enough tidal heating that the formation of chaos terrain by melt-through of a thin conducting ice shell is plausible provided that a mechanism exists which can transmit modest local or regional concentrations of heat from the base of the seafloor to the base of the ice shell. Furthermore, we show

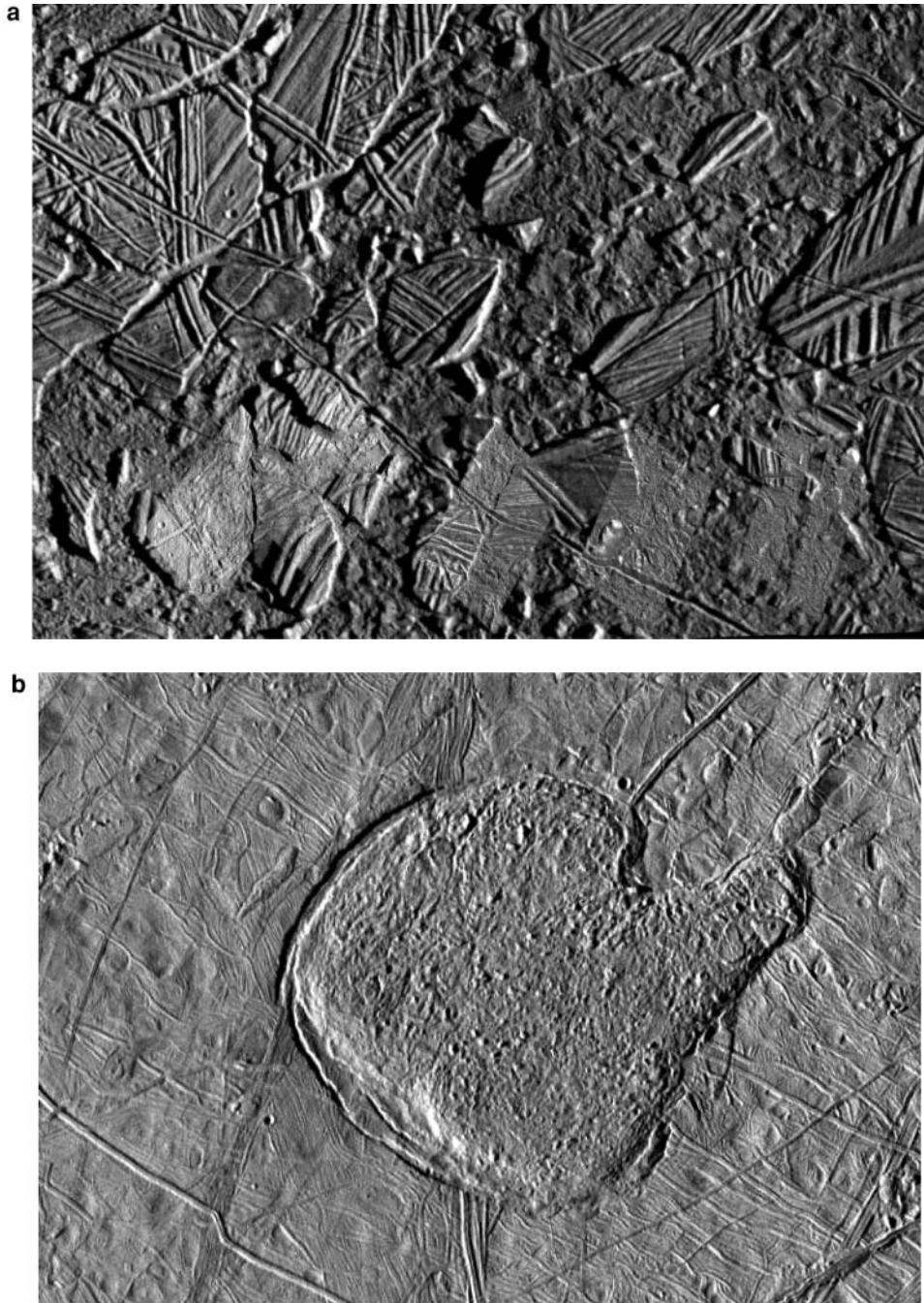


FIG. 1. Examples of chaos terrain on Europa. Figure 1a (40 km across) is a close-up view of Conamara Chaos showing rafts of preexisting material in a broken-up matrix. Figure 1b (175 km across) is the “Mitten,” a chaos region in which nearly all of the preexisting terrain has been destroyed.

that the viscous flow of ice into the melting region would be too slow to stop the melt-through.

2. INTERNAL HEAT GENERATION AND THE STATE OF THE ICE SHELL

The equilibrium thickness of Europa’s ice shell is determined by the heating rate in the silicate interior and in the shell itself.

Unlike Io, Europa’s global heat flow has not been measured since insolation at Europa is orders of magnitude larger (tens of W m^{-2}) than the highest possible surface flux due to internal heating. An estimate of Europa’s internal heating can be obtained by scaling the measured tidal heating rate of Io (10^{14} W) to Europa’s orbital and physical parameters, assuming the same value of the globally effective dissipation parameter Q and potential Love Number k_2 . For a uniform spherical satellite in an

eccentric orbit around Jupiter, the global dissipation rate given by Cassen *et al.* (1980)

$$\dot{E} = \frac{21}{2} G M_J^2 \frac{k_2}{Q} \frac{R_s^5 e^2 n}{a^6}, \quad (1)$$

where G is the gravitational constant, M_J is the mass of Jupiter, and R_s , e , a , and n are the radius, eccentricity, semi-major axis, and mean motion of the satellite. Equation (1) can be used to scale Io's dissipation to Europa

$$\dot{E}_e = \dot{E}_i \left(\frac{R_e}{R_i} \right)^5 \left(\frac{e_e}{e_i} \right)^2 \left(\frac{a_i}{a_e} \right)^6 \frac{n_e}{n_i}. \quad (2)$$

R , a , and e for Io are 1821 km, 4.2×10^5 km, and 0.0041, respectively, and R , a , and e for Europa are ~ 1450 km, 6.7×10^5 km, and 0.010, respectively. R for Europa is given for its silicate interior, rather than the entire satellite, and the fraction n_e/n_i is 0.5 due to the Laplace resonance. This gives a peak heat generation rate in Europa's interior of 5.7×10^{12} W, corresponding to a heat flux through the ice layer (satellite radius of 1560 km) of 0.19 W m^{-2} .

There are two possible modes in which the ice shell can transport this heat. In a "thick" shell, heat is transported through the shell by solid-state convection, and in a "thin" shell, heat is transported by conduction. The actual mode of heat transport is not known, and may depend on the thermal history of Europa, physical parameters, or other factors not considered here. For our modeling, we consider what might happen if the shell is in a conductive state.

The equilibrium thickness h of a conductive ice shell for a heat flux F of 0.19 W m^{-2} can be estimated from the one-dimensional version of Fourier's law to be

$$h \approx k \left(\frac{\Delta T}{F} \right) \approx 3 \text{ km}, \quad (3)$$

where k is the thermal conductivity of ice (around $3.5 \text{ W m}^{-1} \text{ K}^{-1}$) and ΔT is the difference in temperature between the base of the ice (273 K) and the surface (around 100 K). A more exact numerical calculation incorporating temperature dependence of k is done in the following section. The actual thickness may vary over the shell in response to regional variations in the internal heating rate and surface temperature—the equilibrium value of the thickness merely represents the average thickness resulting from an assumed background value of the heat flux from the interior. Any tidal heating which occurs in the shell itself would reduce the average thickness even further.

Such direct scaling of Io's heat flux to Europa's is only valid if the interior states of the two bodies are similar. Geissler *et al.* (2001) argue that Europa, like Io, may have an interior which is partially melted to a degree which maximizes its tidal dissipation. Using a Maxwell viscoelastic model which explicitly includes the temperature dependence of viscosity and rigidity,

they find that the actual peak heating rate is a factor of 1.5 larger than the value obtained by assuming that Europa has the same Q and k_2 values as Io, resulting in a heating rate of 9×10^{12} W, a peak surface heat flux of 0.29 W m^{-2} , and an equilibrium conductive shell thickness h of around 2 km. In addition, the partial melting of the interior that occurs would likely lead to silicate volcanism, which could potentially concentrate heat and lead to local thinning and melting of regions of the shell.

To be conservative, we adopt a global heat flow from the silicate layer of 3×10^{12} W (one-half to one-third of the values predicted above) giving a background value of the heat flux through the ice shell F_{bg} of 3×10^{12} W, which is consistent with an equilibrium conductive ice shell thickness h of around 6 km. Based on numerical experiments, McKinnon (1999) argues that a conductive ice shell less than 10 km thick is stable against convection for even the lowest possible melting-point viscosity. For higher melting-point viscosities, this transition thickness is even larger.

3. MELTING MODEL

In order to examine possible melt-through we developed a numerical simulation that calculates the time-varying temperature profile and tracks melting in an ice shell resulting from a heat concentration. This heat concentration is assumed to be axisymmetric and Gaussian in profile, and is superimposed on a uniform background heat flux F_{bg} . The temperature dependence of the thermal conductivity and heat capacity of ice are explicitly included, as well as tidal heating within the shell, heat from the interior, and the latent heat of fusion of ice. Heat is transferred by conduction within the ice shell.

In the numerical model, the region of the shell in question is divided into many ringlike cells in the radial and vertical direction (Fig. 2). The heat ΔQ absorbed by or removed from a given cell during a given time step Δt can be found by solving the heat conservation equation in response to (a) the heat flux $\mathbf{F}(t)$ through the cell and (b) heat generation per unit volume q within the cell due to tidal flexing of the shell

$$\Delta Q = \left[\oint \mathbf{F}(t) \cdot d\mathbf{s} + qV \right] \Delta t, \quad (4)$$

where the density of ice $\rho_i = 940.0 \text{ kg m}^{-3}$, V is the cell volume, and \mathbf{s} is the surface normal vector pointing into the cell. The temperature change of the cell is then

$$\Delta T = \frac{\Delta Q}{\rho_i V c_p}, \quad (5)$$

where c_p is the heat capacity of ice at constant pressure. The heat capacity is temperature dependent, going as

$$c_p(T) = a_1 T + a_0, \quad (6)$$

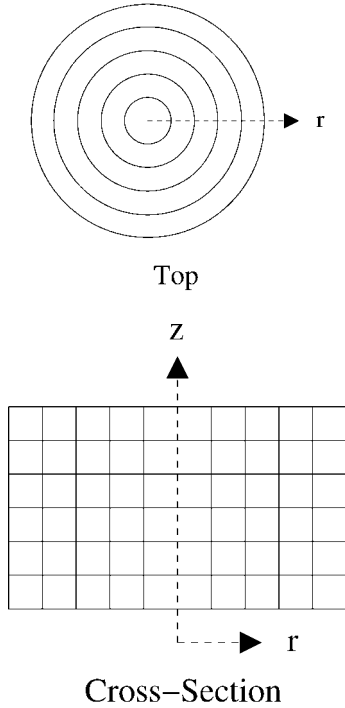


FIG. 2. Schematic showing the grid used for the numerical thermal model. The grid is divided into cells in the radial and vertical direction, as shown in the cross section. Because the model is axisymmetric, the azimuthal coordinate is not considered and the individual cells form rings as shown in the top view.

with $a_1 = 7.037 \text{ J kg}^{-1} \text{ K}^{-2}$ and $a_0 = 185 \text{ J kg}^{-1} \text{ K}^{-1}$ (Dorsey 1940). In the case where a cell is at the melting point, its temperature does not change. Instead, it will be in a process of gaining or losing latent heat. In this case, we keep track of the latent heat (per unit mass) L which the cell has absorbed

$$\Delta L = \frac{\Delta Q}{\rho_i V}. \quad (7)$$

When the latent heat absorbed by a cell equals or exceeds the latent heat of fusion of ice ($3.35 \times 10^5 \text{ J kg}^{-1}$), the cell is considered melted and removed from the grid.

The flux across a given cell face may be due to heat from the interior, in the case of the cell at the base of the shell, or the absorption or emission of thermal radiation at the surface of the shell. For most cell faces, however, the heat flux is a result of the temperature gradient between neighboring cells (taken in the direction of the inward surface normal vector \hat{s}), and is given by Fourier's law,

$$\mathbf{F}_{\text{face}} = -k \nabla_s T, \quad (8)$$

where k is the thermal conductivity of ice. Like heat capacity, k is temperature dependent,

$$k(T) = \frac{b_1}{T} + b_0, \quad (9)$$

with $b_1 = 4.88 \times 10^2 \text{ W m}^{-1}$ and $b_0 = 4.68 \times 10^{-1} \text{ W m}^{-1} \text{ K}^{-1}$ (Hobbs 1974). For the lower face of cells at the base, \mathbf{F}_{face} is set to the assumed basal heat flux (the uniform background value plus the heat concentration). For the upper face of the cells at the surface, the net flux is the difference between the incoming solar flux and the radiated blackbody flux

$$\mathbf{F}_{\text{surf}} = \mathbf{F}_{\text{solar}} - \sigma_s T_{\text{surf}}^4 \hat{s}, \quad (10)$$

where σ_s is the Stefan–Boltzmann constant and \hat{s} is the unit surface normal vector pointing into the cell. We use the expressions for the diurnally averaged solar flux as a function of colatitude ϕ derived by Ojakangas and Stevenson (1988)

$$\mathbf{F}_{\text{solar}} = (1 - A) F_s \frac{\sqrt{i^2 + \phi^2}}{\sqrt{2\pi}} \hat{s} \quad (\phi < i) \quad (11a)$$

$$\mathbf{F}_{\text{solar}} = (1 - A) F_s \frac{\sin \phi}{\pi} \hat{s} \quad (i < \phi < \pi - i) \quad (11b)$$

$$\mathbf{F}_{\text{solar}} = (1 - A) F_s \frac{\sqrt{i^2 + (\pi - \phi)^2}}{\sqrt{2\pi}} \hat{s} \quad (\phi > \pi - i), \quad (11c)$$

where i is Europa's obliquity, approximately 0.05 radians (3°); A is the albedo, roughly 0.5; and F_s is the solar flux at Jupiter, approximately 50.0 W m^{-2} . The surface areas of each cell face, along with the heat flux calculated at each cell face, are used to calculate the integrals of the flux \mathbf{F} over the surface of each cell in Eq. (4).

The term q in Eq. (4) is due to tidal dissipation within the shell itself. The total heat generation within the shell is small compared to the assumed heat generation within the silicate interior, but we include it in our model for completeness. The tidal heating calculations for the shell in our model follow that of Ojakangas and Stevenson (1989). It is assumed that the ice behaves as a Maxwell viscoelastic medium in which the volumetric heating rate q can be expressed in terms of the rigidity μ , viscosity η , strain rates in the shell $\dot{\epsilon}_{ij}$, and forcing frequency ω as

$$q = \frac{2\mu \overline{\dot{\epsilon}_{ij}^2}}{\omega} \left[\frac{\omega \tau_M}{1 + (\omega \tau_M)^2} \right], \quad (12)$$

where ω is equal to Europa's mean motion $n = 2.05 \times 10^{-5} \text{ sec}^{-1}$, $\mu = 4 \times 10^9 \text{ Pa}$, and τ_M is the Maxwell time η/μ . $\overline{\dot{\epsilon}_{ij}^2}$ signifies the sum of the time-averaged squares of the individual components of the strain rate tensor $\dot{\epsilon}_{ij}$, which can be obtained from the relations derived in Ojakangas and Stevenson (1989) and is a function of position on the shell. Its value ranges from around $10^{-21} \text{ sec}^{-2}$ near the sub-Jupiter point to around $7 \times 10^{-20} \text{ sec}^{-2}$ near the poles. The viscosity η is defined by an Arrhenius relation

$$\eta(T) = \eta_o \exp \left[l \left(\frac{T_m}{T} - 1 \right) \right], \quad (13)$$

where T_m is the melting point of ice (273 K), $l \approx 27$, and the melting point viscosity $\eta_o \approx 10^{14}$ Pa s (Turcotte and Schubert 1982). These values give a volumetric heating rate q of around 10^{-5} W m $^{-3}$ in the warm ice at the base of the shell. This heating rate drops off rapidly in the cooler ice above. Ojakangas and Stevenson (1989) also considered the dissipation rate which results from using Glen's flow law, a non-Newtonian rheology for ice, and found that the dissipation is comparable to that obtained using the Maxwell model.

The basal heat flux concentration applied on top of the background value of the heat flux F_{bg} is modeled as a Gaussian with maximum flux F_o and a radial extent described by the scale width d_o :

$$\mathbf{F}_{\text{base}} = F_o \exp\left(-\frac{8r^2}{d_o^2}\right) \hat{\mathbf{s}} + F_{bg} \hat{\mathbf{s}}. \quad (14)$$

The scale width d_o is defined such that the heat flux drops to a fraction e^{-2} (14%) at a radius $d_o/2$ from the center. It effectively defines the diameter of the heat flux concentration. The total power P_o of the heat concentration must equal the area integral of the additional heat flux

$$P_o = \int_0^\infty \int_0^{2\pi} F_o \exp\left(-\frac{8r^2}{d_o^2}\right) r \, d\theta \, dr. \quad (15)$$

Solving this for the constant F_o gives

$$F_o = \frac{8P_o}{\pi d_o^2}. \quad (16)$$

Thus, if we specify P_o and d_o for a given case, F_o is given by Eq. (16).

4. NUMERICAL EXPERIMENTS

We have modeled melt-through events for a wide range of Gaussian heat concentrations defined by total power P_o and scale width d_o . The assumed background heat flux F_{bg} is 0.1 W m $^{-2}$ in all cases, and the position on the shell is chosen to be the sub-Jupiter point for calculation of the surface temperature of the shell and the dissipation within the shell [Eqs. (11a), (11b), (11c), and (12)]. Varying the position on the shell results in no more than a 25% change in the equilibrium shell thickness and melt-through time scales which we calculate.

With the relations and boundary conditions from Section 3, we solve first for the equilibrium state of the ice shell. We start with a grid with radius d_o that is thicker than the expected equilibrium thickness and apply a linear temperature profile to it. The radial and vertical dimension of the cells (Δr and Δz) is 100 m. The heat flux at the base of the shell F_{base} is set to the assumed background value $F_{bg} = 0.1$ W m $^{-2}$ (about a third of the maximum value calculated in Section 2) and for each time step we loop over each cell calculating its change in temperature. The time step (Δt) is chosen to be 1/10 of the thermal diffusion time

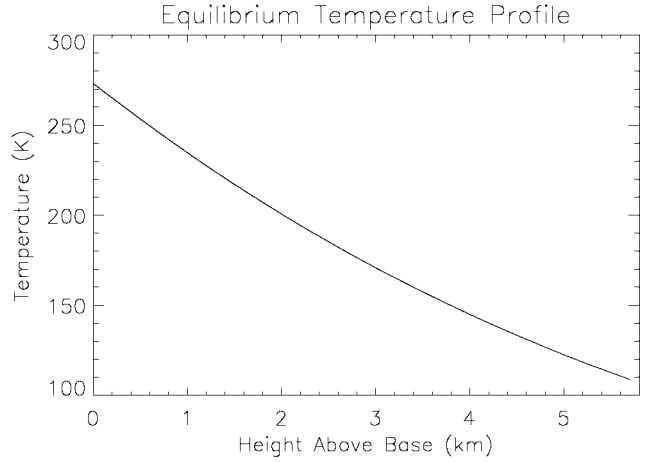


FIG. 3. Equilibrium temperature profile of the shell at the sub-Jupiter point, which is the position of our numerical melt-through studies. The basal temperature is 273 K and the surface temperature is about 110 K. The curvature of the temperature profile is due primarily to the temperature-dependent thermal conductivity of ice.

($\Delta t = \rho_i c_p \Delta z^2 / 10k = \rho_i c_p \Delta r^2 / 10k$). Cells which melt away from the base are removed. This process eventually converges to a steady state and allows us to extract both the equilibrium shell thickness and the equilibrium temperature profile in the shell. Figure 3 shows the temperature profile of the shell, which has an equilibrium thickness of 5.8 km.

Once the equilibrium temperature profile is achieved, a range of heat concentrations defined by P_o and d_o are applied to the base of the shell. The time step is now chosen such that the base cells absorb no more than 1/10 of their total latent heat in a given time step ($\Delta t = \rho_i Q_{\text{latent}} \Delta z / 10F_o$), which is significantly shorter than the thermal diffusion time. Figures 4 and 5 show the progression of heating and melting resulting from heat concentrations of 5×10^{10} W and 5×10^{11} W, respectively, each with d_o of 200 km describing their lateral extent. These heat concentrations correspond to about 2 and 15%, respectively, of Europa's total heating rate assumed here. For comparison, the largest volcano on Io (Loki) emits about 30% of Io's total internal heat. The final melt-through diameter in each case is about 90 km, which is reached after 40,000 years in the 2% case and only 4000 years in the 15% case. The temperature distributions in all cases are similar, but in the higher heating cases the isotherms become more compressed around the melt cavity. A case with a more confined heat concentration (d_o of 100 km) is shown in Fig. 6 for a total power P_o of 5×10^{10} W (same power as the case in Fig. 4). This case results in a melt-through about 45 km in diameter after 10,000 years.

The results of the full range of numerical experiments we have performed is summarized in Figs. 7 and 8. Figure 7 shows the radii of melt-throughs which result from heat concentrations P_o of 5×10^{10} W as a function of time for d_o of 20, 40, 60, 100, 150, and 200 km. Figure 8 shows similar results for P_o values of 5×10^{11} W. For strong, localized heat concentrations,

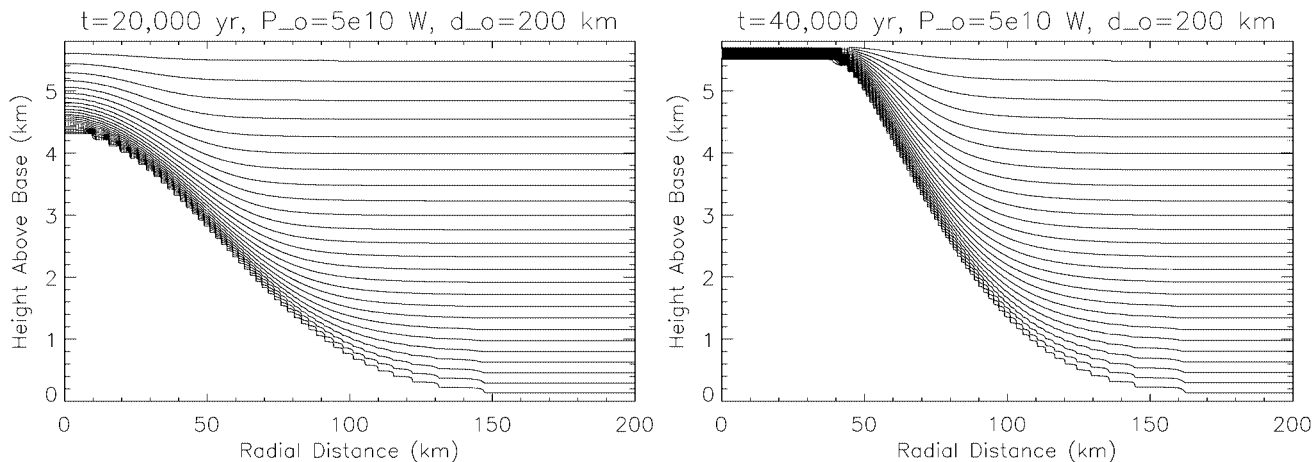


FIG. 4. Isotherm plots of the melt progression resulting from a heat source applied at the base of the shell with a total power 5×10^{10} W distributed as a Gaussian with a scale width d_o of 200 km. The base of the shell is at 273 K, the surface is around 110 K, and the isotherms are spaced by about 8° K. The total applied power is only about 2% of Europa's total internally generated heat.

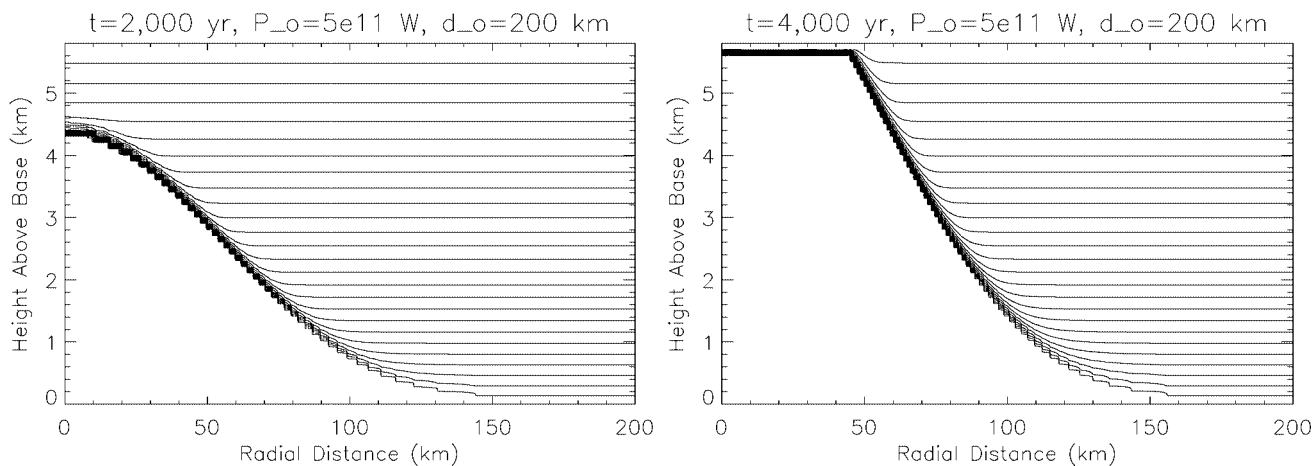


FIG. 5. Same as Fig. 4 except that the total power applied is increased to 5×10^{11} W.

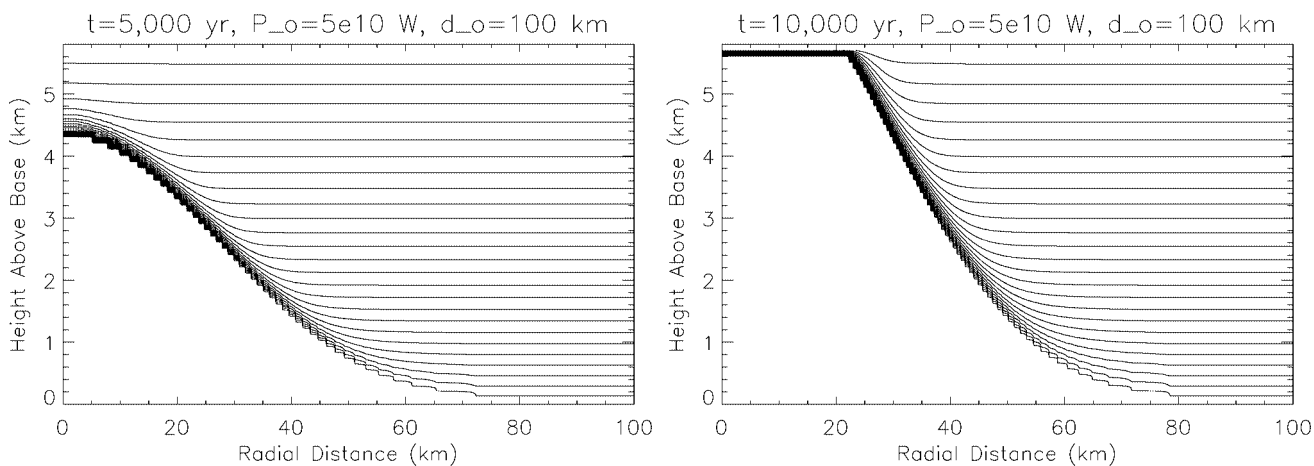


FIG. 6. Same as Fig. 4 except that d_o has been reduced to 100 km.

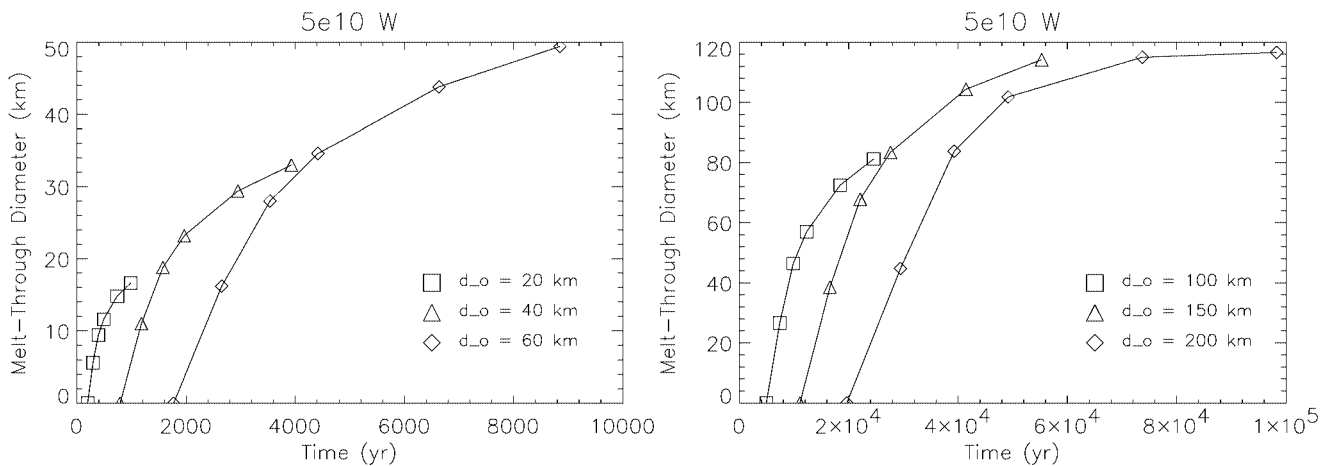


FIG. 7. Compilation of the results of numerical melt-through simulations for a heat source of 5×10^{10} W (about 2% of Europa's internally generated heat) and scale width d_o of 20, 40, 60, 100, 150, and 200 km. Melt-through radius is given as a function of time and d_o .

melt-through can occur in a few hundred years. Significant melt-through occurs very quickly in all of the cases studied here, and the melt times vary as P_o^{-1} and d_o^2 , which are physically reasonable dependences.

5. IN-FLOW OF ICE

In order for melting to progress, the rate of melting must outpace the flow of ice back into the region. An isostatically compensated shell with a locally thin region develops a pressure gradient which drives ice flow into the thin region as shown in Fig. 9. In the simulations in Section 4 we assumed that this flow rate is negligible. Here, we calculate the flow rates which would occur in the ice shell as it thins. We use the temperature and thickness profiles we have calculated for each of the melt-through scenarios in Section 4. This analysis follows that of

Stevenson (2000), who approximated the flow of ice as a 2D horizontal channel flow rather than a radial flow. Here, however, we explicitly treat the fact that the flow into a melting region is radially symmetric. The horizontal pressure gradient due to the local thinning of the shell is

$$\frac{dP(r)}{dr} = (\rho_w - \rho_i)g \frac{\rho_i}{\rho_w} \frac{dD(r)}{dr}, \quad (17)$$

where r is the radial direction, z is positive upward, $D(r)$ is the thickness, $\rho_w = 1000 \text{ kg m}^{-3}$, and $\rho_i = 940 \text{ kg m}^{-3}$. This pressure gradient drives a flow along the base of the ice with horizontal velocity $u(r, z)$, which can be described by a Pouseuille flow law

$$\frac{dP(r)}{dr} = \frac{d}{dz} \left(\eta(r, z) \frac{du(r, z)}{dz} \right), \quad (18)$$

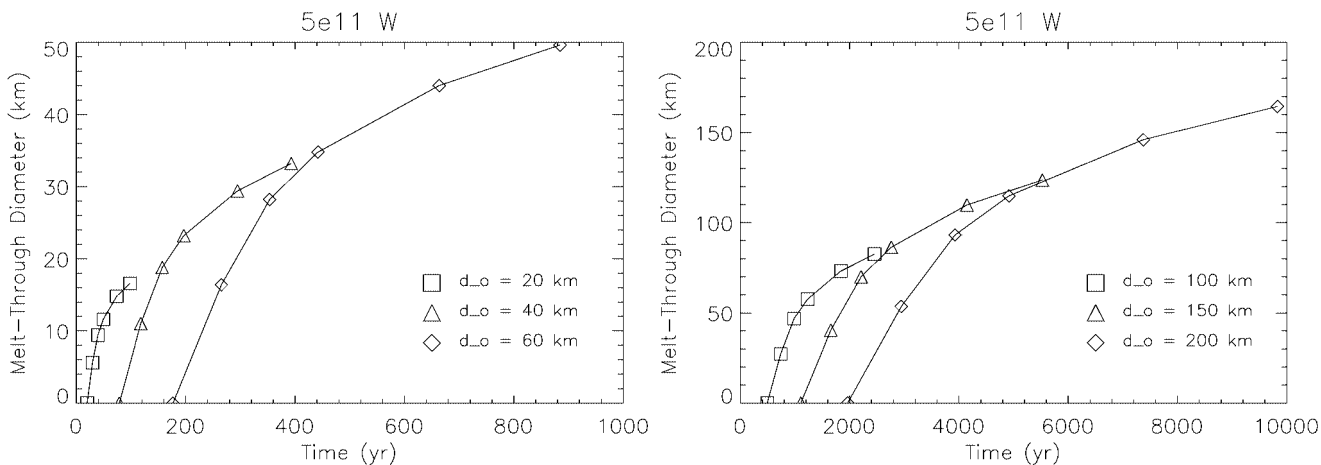


FIG. 8. Same as Fig. 7 except that the total power applied is increased to 5×10^{11} W.

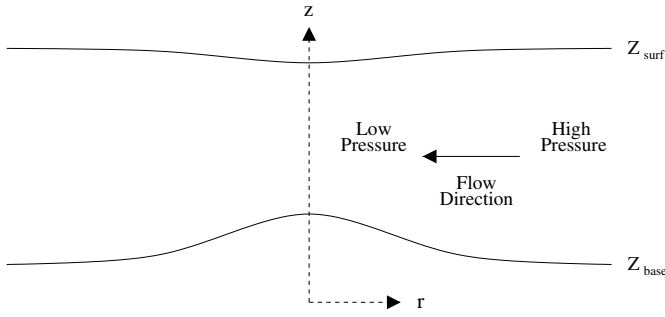


FIG. 9. Schematic showing pressure differential and resulting flow direction in an isostatically compensated shell which has an axisymmetric local thinning.

where η is the viscosity defined in Eq. (13), which varies exponentially with temperature and, therefore, roughly exponentially with z .

Taking the temperature profiles and thicknesses obtained from the thermal model and assuming isostasy, we numerically integrate Eq. (18) with a free-slip boundary condition at the base, since the ocean applies no shear stress to the shell, and a zero-velocity boundary condition at the upper surface, where the viscosity is high enough to prevent the flow of ice

$$\left. \frac{du(r, z)}{dr} \right|_{z=Z_{\text{base}}} = 0 \quad (19a)$$

$$u(r, z_{\text{surf}}) = 0. \quad (19b)$$

This integration gives the velocity profile $u(r, z)$ at a given radius. Because of continuity, the rate of change of the ice thickness at a given location is given by the divergence of the depth-integrated velocity $U(r)$

$$\frac{dD(r)}{dt} = -\frac{1}{r} \frac{d}{dr}(rU(r)) = -\frac{U(r)}{r} - \frac{dU(r)}{dr}, \quad (20)$$

where

$$U(r) = \int_{z_{\text{base}}}^{z_{\text{surf}}} u(r, z) dz. \quad (21)$$

Figure 10 shows the depth-integrated velocity vs. radial distance for the case where the total applied power P_o is 5×10^{10} W and the scale width d_o of the heat source is 200 km. Figure 11 shows the thickening rate vs. radial distance which results from this ice flow. The calculation is done when the shell has thinned by about 1 km. The peak thickening rate in this case is around 8×10^{-5} m yr $^{-1}$, which is orders of magnitude lower than the peak melting rate of 0.27 m yr $^{-1}$. The term $U(r)/r$ in Eq. (20) is due to the use of polar coordinates, and would be expected to become significant near the center of the melting region. However,

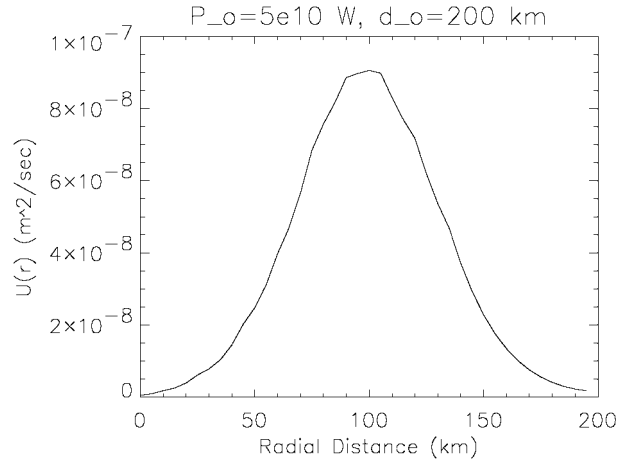


FIG. 10. Depth integrated velocity $U(r)$ of the ice flow into the melting region. This plot is for the case where the total power applied to melt the shell P_o is 5×10^{10} W and the scale width d_o is 200 km. The flow velocity is calculated when about 1 km of ice has been melted away.

the flow velocities are small enough that this term makes a negligible contribution to the thickening rate, even toward the center.

Figure 12 shows the rates of melting and of thickening due to ice flow for a total power P_o of 5×10^{10} W (2% of the total assumed heat production) and a range of scale widths d_o . These values are calculated when the shell has thinned by about 1 km. In all cases, melting outpaces thickening due to ice flow by orders of magnitude. The rates of thickening due to ice flow do not significantly increase as the shell becomes thinner even though thinning results in a higher pressure gradient to drive ice flow. As melting progresses, warm ice is melted away from the bottom layer before it can appreciably conduct heat to the colder ice above (seen in Figs. 4 through 6 as a squeezing together of the isotherms). The decrease in the amount of warm ice capable of flow offsets the increased pressure gradient resulting from

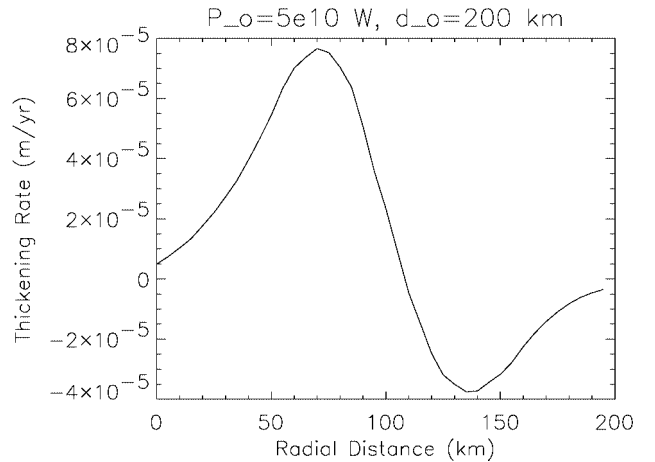


FIG. 11. Rate of thickening of the shell due to the ice flow in Fig. 10. The peak thickening rate here is orders of magnitude lower than the peak rate of thinning of the shell due to melting (0.27 m yr $^{-1}$).

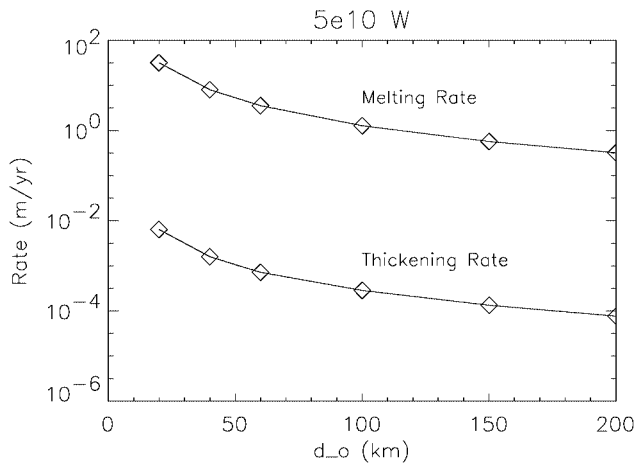


FIG. 12. Comparison of the rates of thinning of the shell due to melting and thickening of the shell due to ice flowing into the melting region for a total applied power of 5×10^{10} W and a range of scale widths d_o . In all cases, the melting rate is orders of magnitude greater than the thickening rate due to ice flow.

thinning. Increasing the total power by an order of magnitude increases the melting rate by an order of magnitude and decreases the thickening rate since even less heat is conducted upward into the colder ice (more compressed isotherms). Decreasing the melting point viscosity of ice η_o in Eq. (13) from 10^{14} to 10^{13} Pa s, which is a reasonable lower limit for the melting point viscosity of ice (McKinnon 1999) causes the thickening rate to increase by an order of magnitude, but the melting rates are still orders of magnitude larger than the thickening rates.

In contrast to the results of Stevenson (2000), who implicitly assumed a thick ice shell, flow of ice is unimportant in a thin conducting shell. In a thin shell there is only a very thin layer of ice at the base of the shell, which has a low enough viscosity to appreciably flow. Furthermore, as melting progresses, the cold ice above the melting region is not appreciably heated, so the amount of warm ice capable of flowing decreases. Thicker shells (tens of km) would have a correspondingly thicker layer of ice which can flow, especially in the case of a convective shell where a large layer of the shell would be within a few tens of degrees of the melting point.

6. SUMMARY AND DISCUSSION

Given the possibility that tidal heating in the silicate interior of Europa is significant, a thin shell and seafloor heat concentrations are plausible. Provided that there is a mechanism to transmit these heat concentrations to the base of the ice shell, frequent melt-through events on Europa are possible and will occur faster than the viscous inflow of ice can counteract them. This result supports the interpretation of Greenberg *et al.* (1999) and Riley *et al.* (2000) that the widespread chaos features found on Europa are the result of melt-through.

The maximum possible steady-state heat flux from the interior results in a shell approximately 2 km in thickness. The

steady-state flux assumed here is about a third of the maximum, resulting in a shell about 6 km in thickness—still well below the thickness for which solid-state convection could set in. The heat is likely to be concentrated in some locations due to silicate volcanism or hot spots at the ocean-mantle interface. A few percent of Europa's predicted internal heat concentrated over an area 200 km in diameter can result in melt-through 90 km in diameter within 40,000 years. Concentrations of tens of percent of Europa's heat over a smaller area can create 10–20 km diameter melt-throughs within a few hundred years. In contrast to the results of Stevenson (2000), the flow of ice at the base of a thin shell is negligible compared to the removal of ice by melting, such that it is incapable of significantly slowing the melt-through event.

Our model is based upon the assumption that heat concentrations occur on Europa and are capable of affecting the shell. There are several proposed ways for these heat concentrations to occur. Volcanic activity at the base of the ocean is plausible, given the large predicted heat flux from the interior, and could lead to significant concentrations of the internally generated heat, like volcanism does on Io. Provided that the ocean is not strongly stratified, e.g., due to turbulent convection, thermal plumes driven by these volcanos or hot spots may propagate to the base of the shell through the ocean with minimal dispersion (Thomson and Delaney 2001). If the ocean is hot and significantly stratified, the possibility exists for catastrophic turnover or strong convective plumes which could lead to large heat concentrations at the base of the shell (Kargel *et al.* 2000). Further research and in-situ experiments are necessary to determine the nature, source, and plausibility of heat concentrations on Europa and to determine if they are consistent with the observed size distribution and morphology of chaos regions.

While we assume a smooth distribution for the heat concentration and no initial topography on the shell in our model, in reality, neither the heat source nor the shell are perfectly uniform. There will be local variations in the thickness of the shell due to topography, such as ridges, as well as small-scale variations in the heating due to currents and turbulence in the ocean. As a region of the shell thins in response to a melt-through event, tidal stresses may lead to cracking and breakup of that region of the shell. Thicker regions of the shell are more likely to survive as rafts in the chaos region, while the remainder of the preexisting terrain is destroyed. The duration and strength of the heating event determines the degree to which preexisting terrain is destroyed, and therefore the final appearance of the chaos region. Likewise, preexisting topography and small-scale turbulence may cause a large heat concentration to produce a cluster of small melt-throughs rather than a single large melt-through.

Future missions to Europa may be able to observe features of chaos regions which are not obtainable from current observations, possibly determining if they are indeed formed by melt-through. In our model, chaos regions can be formed by melt-through on time scales from hundreds of years to tens of thousands of years. The time for refreezing of melt-through

regions may be significantly longer, ~ 1 M yr (Thomas *et al.* 2000). Thermal imaging could detect sites where ice is freezing over a body of water for a few 100 years (Van Cleve *et al.* 1999), and might reveal any chaos regions that are very recent in origin. Radar sounding of Europa's shell, planned for the future Europa Orbiter, could detect local thinning of the ice shell. Given the longer time scale for refreezing of the ice than for melt-through, radar sounding is more likely to detect locally thin ice under a chaos region which is in the refreezing process than one which is in the melting process. The radar may be able to determine whether the region is in the process of melting or refreezing, based on the character of the ice. Either way, detection of local thinning, especially if correlated with hot spots detected by thermal imaging, would be a strong indicator of on-going melt-through on Europa.

If melt-through occurs, as we propose, it could provide an important link between the ocean and the surface. Melt-through would be significant from an astrobiological perspective in that chemical compounds (both organic and inorganic) delivered to or created at the surface can be incorporated into the crust and ocean (Greenberg *et al.* 2000). Moreover, it might play an important role in the lifecycle of organisms existing in Europa's shell. From an exploratory perspective, chaos regions which have recently refrozen, as determined by radar sounding and/or thermal imaging, may provide an indication of the oceanic composition by remote sensing. For lander missions, fresh chaos regions may be good locations for taking samples or attempting to penetrate through the shell to obtain samples from the ocean.

ACKNOWLEDGMENTS

The authors thank Richard E. Thomson and Jeff Kargel for their helpful reviews and comments. This work was supported by a grant from the NSF Life in Extreme Environments program. David O'Brien is supported by a NASA GSRP fellowship.

REFERENCES

- Carr, M. H., M. J. S. Belton, C. R. Chapman, M. E. Davies, P. Geissler, R. Greenberg, A. S. McEwan, B. R. Tufts, R. Greeley, and R. Sullivan 1998. Evidence for a subsurface ocean on Europa. *Nature* **391**, 363.
- Cassen, P., R. T. Reynolds, and S. J. Peale 1979. Is there liquid water on Europa? *Geophys. Res. Lett.* **6**, 731–734.
- Cassen, P., S. J. Peale, and R. T. Reynolds 1980. Tidal dissipation on Europa—A correction. *Geophys. Res. Lett.* **7**, 987–988.
- Collins, G. C., J. W. Head, R. T. Pappalardo, and N. A. Spaul 2000. Evaluation of models for the formation of chaotic terrain on Europa. *J. Geophys. Res.* **105**, 1709–1716.
- Dorsey, N. E. 1940. *Properties of Ordinary Water-Substance in all its Phases: Water-Vapor, Water, and all the Ices*. Reinhold, New York.
- Geissler, P., D. P. O'Brien, and R. Greenberg 2001. Silicate volcanism on Europa. *Lunar Planet. Sci.* **32**, Abstract 2068.
- Greeley, R., and 20 colleagues 1998. Europa: Initial Galileo geological observations. *Icarus* **135**, 4–24.
- Greenberg, R., P. Geissler, G. V. Hoppa, B. R. Tufts, D. D. Durda, R. Pappalardo, J. W. Head, R. Greeley, R. Sullivan, and M. H. Carr 1998. Tectonic processes on Europa: Tidal stresses, mechanical response, and visible features. *Icarus* **135**, 64–78.
- Greenberg, R., G. V. Hoppa, B. R. Tufts, P. Geissler, J. Riley, and S. Kadel 1999. Chaos on Europa. *Icarus* **141**, 263–286.
- Greenberg, R., P. Geissler, B. R. Tufts, and G. V. Hoppa 2000. (E)Habitability of Europa's crust: The role of tidal-tectonic processes. *J. Geophys. Res.* **105**, 17551–17562.
- Head, J. W., and R. T. Pappalardo 1999. Brine mobilization during lithospheric heating on Europa: Implications for formation of chaos terrain, lenticulae texture, and color variations. *J. Geophys. Res.* **104**, 27143–27155.
- Hobbs, P. V. 1974. *Ice Physics*. Clarendon Press, Oxford.
- Hoppa, G. V., B. R. Tufts, R. Greenberg, and P. Geissler 1999. Strike-slip faults on Europa: Global shear patterns driven by tidal stress. *Icarus* **141**, 287–298.
- Kargel, J. S., J. Z. Kaye, J. W. Head, III., G. M. Marion, R. Sassen, J. K. Crowley, O. P. Ballesteros, S. A. Grant, and D. L. Holgenboom 2000. Europa's crust and ocean: Origin, composition, and the prospects for life. *Icarus* **148**, 226–265.
- McKinnon, W. B. 1999. Convective instability in Europa's floating ice shell. *Geophys. Res. Lett.* **26**, 951–954.
- Ojakangas, G. W., and D. J. Stevenson 1989. Thermal state of an ice shell on Europa. *Icarus* **81**, 220–241.
- Pappalardo, R. T., J. W. Head, R. Greeley, R. J. Sullivan, C. Pilcher, G. Schubert, W. B. Moore, M. H. Carr, J. M. Moore, and M. J. S. Belton 1998. Geological evidence for solid-state convection in Europa's ice shell. *Nature* **391**, 395.
- Pappalardo, R. T., and 31 colleagues 1999. Does Europa have a subsurface ocean? Evaluation of the geological evidence. *J. Geophys. Res.* **104**, 24015–24056.
- Riley, J., G. V. Hoppa, R. Greenberg, B. R. Tufts, and P. Geissler 2000. Distribution of chaotic terrain on Europa. *J. Geophys. Res.* **105**, 22599–22616.
- Spaul, N. A., J. W. Head, G. C. Collins, L. M. Prockter, R. T. Pappalardo 1998. Conamara Chaos region, Europa: Reconstruction of mobile polygonal ice blocks. *Geophys. Res. Lett.* **25**, 4277.
- Squyres, S. W., R. T. Reynolds, and P. M. Cassen 1983. Liquid water and active resurfacing on Europa. *Nature* **301**, 225–226.
- Stevenson, D. J. 2000. Limits on the variation in thickness of Europa's ice shell. *Lunar Planet. Sci.* **32**, Abstract 1506.
- Thomas, P. J., M. R. Goulet, A. J. Smith, D. G. B. Whitelaw, and C. F. Chyba 2000. Refreezing timescales following a melt-through event on Europa. *Lunar Planet. Sci.* **32**, Abstract 1208.
- Thomson, R. E., and J. R. Delaney 2001. Evidence for a weakly stratified European ocean sustained by seafloor heat flux. *Lunar Planet. Sci.* **32**, Abstract 1347.
- Tufts, B. R., R. Greenberg, G. V. Hoppa, and P. Geissler 2000. Lithospheric dilation on Europa. *Icarus* **146**, 75–97.
- Turcotte, D. L., and G. Schubert 1982. *Geodynamics: Applications of Continuum Physics to Geological Problems*. Wiley, New York.
- Van Cleve, J. E., R. T. Pappalardo, and J. R. Spencer 1999. Thermal palimpsests on Europa: How to detect sites of current activity. *Lunar Planet. Sci.* **32**, Abstract 1815.
- Zahnle, K., L. Dones, and H. F. Levison 1998. Cratering rates on the Galilean satellites. *Icarus* **136**, 202–222.